Accepted Manuscript

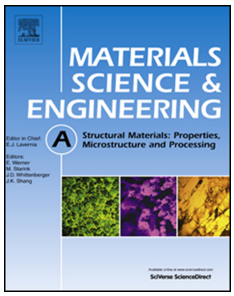

Assessment of the potential of hydrogen plasma charging as compared to conventional electrochemical hydrogen charging on dual phase steel

T. Depover, T. Hajilou, D. Wan, D. Wang, A. Barnoush, K. Verbeken

PII: S0921-5093(19)30410-1

DOI: https://doi.org/10.1016/j.msea.2019.03.097

Reference: MSA 37714

To appear in: *Materials Science & Engineering A*

Received Date: 10 October 2018

Revised Date: 19 March 2019

Accepted Date: 21 March 2019

Please cite this article as: T. Depover, T. Hajilou, D. Wan, D. Wang, A. Barnoush, K. Verbeken, Assessment of the potential of hydrogen plasma charging as compared to conventional electrochemical hydrogen charging on dual phase steel, *Materials Science & Engineering A* (2019), doi: https://doi.org/10.1016/j.msea.2019.03.097.

Assessment of the potential of hydrogen plasma charging as compared to conventional electrochemical hydrogen charging on dual phase steel

T. Depover[1], T. Hajilou[2], D. Wan[2], D. Wang[2], A. Barnoush[2] and K. Verbeken[1]

[1]*Department of Materials, Textiles and Chemical Engineering, Ghent University (UGent), Technologiepark 903, B-9052 Ghent, Belgium*

[2]*Department of Mechanical and Industrial Engineering, Norwegian University of Science and Technology (NTNU), Richard Birkelands vei 2, 7491 Trondheim, Norway*

Corresponding author:
Tom Depover
Tel.: 32-9-331-0433
E-mail: Tom.Depover@ugent.be

Keywords: Hydrogen embrittlement; Dual phase steel; Hydrogen trapping; Dislocations; Nanoindentation

Abstract

The present study evaluates the hydrogen induced damage by in-situ hydrogen plasma charging in dual phase (DP) steel. Cold deformation of 15% is applied on the material to change microstructural defects, such as dislocation density. The susceptibility to hydrogen embrittlement is hence evaluated for two material conditions, i.e. DP 0% and DP 15%. Small scale tensile tests are done inside an ESEM chamber for which in-situ hydrogen plasma charging is compared with electrochemical hydrogen charging while uncharged samples serve as a reference. Generally, the hydrogen effect on the ductility and stress level is increased when deformation is applied, due to the hydrogen trapping ability of the deformation induced defects, as confirmed by thermal desorption spectroscopy. Complementary in-situ electrochemical nanoindentation tests verify the more pronounced hardness increase due to hydrogen when cold deformation is applied. A slightly increased ductility loss is observed when the samples are charged electrochemically, although similar tendencies are found for both hydrogen charging procedures. These observations are confirmed by the fractographic analysis, where the detrimental role of MnS inclusions in the segregation line on hydrogen induced cracking is demonstrated as well.

1. Introduction

The presence of hydrogen in steels is well-known to be detrimental for the overall performance and more precisely the mechanical properties of the material since ductility decreases and unpredictable failure may occur. Consequently, insight in the interaction between hydrogen and the material remains of crucial importance. For this purpose, researchers have been selecting different methods to charge a specific material with hydrogen and subsequently to compare the material's behavior before, and during or after this charging procedure. For instance, electrochemical hydrogen charging is often applied to evaluate hydrogen trapping, verify the hydrogen saturation level (e.g. depending on the applied charging conditions) and determine the hydrogen induced damage. Hydrogen induced blisters and internal damage might occur when too severe charging conditions are applied. For instance, the appearance of blisters increased with applied charging time and current density, as observed by Pérez Escobar et al. [1, 2]. They performed blister mapping of commercial high strength steels, such

as a dual phase (DP), transformation induced plasticity (TRIP), ferrite bainite (FB) and high strength low alloyed (HSLA) steels. Next to the blister detection, the hydrogen induced cracks were, in the case of DP steel, also demonstrated to be linked to MnS inclusions in the segregation line of DP steel. Other examples of hydrogen/material interaction studies based on electrochemical hydrogen charging can be found in Refs. [3, 4, 5, 6]. Another, regularly used, method to charge a material with hydrogen is H_2 gas. Gaseous hydrogen charging at elevated temperature is for instance a prerequisite to charge incoherent TiC precipitates, as shown by Wei and Tsuzaki [7] and Pérez Escobar et al. [8]. It might also be very efficient to charge face centered cubic (fcc) materials due to its significantly lower hydrogen diffusivity compared to body centered cubic (bcc) metals. More examples can be found in Refs. [9, 10, 11, 12, 13]. Recently, another innovative method was used by Deng et al. [14] and Rogne et al. [15]. They used water vapor to charge Fe-Al intermetallic alloys as H_2O may react with Al, producing both alumina and hydrogen to be absorbed in the matrix.

Furthermore, also the use of in-situ hydrogen charging has proven to be vital to evaluate the hydrogen induced mechanical degradation since due to the high hydrogen diffusion coefficient in bcc steels, an important part of hydrogen will have effused from the sample when ex-situ charging would be applied. Hence, the mobile hydrogen, assumed to be mostly trapped by dislocations, will not be able to play its detrimental role [16, 17, 18, 19, 20, 21]. Up to now, in-situ hydrogen charging is either done during high pressure hydrogen gas or under electrochemical cathodic hydrogen charging. Both charging methods complicate a possible direct high-resolution observation of the sample during deformation by tensile testing.

To take into account the specific nature of high resolution observation, a novel approach was recently developed by Wan et al. [22]. Environmental scanning electron microscopy (ESEM) was combined with small size tensile set-up to test the impact of hydrogen on the mechanical deformation. Nevertheless, the fugacity of hydrogen is not enough at low pressure in ESEM to have adequate physisorption and dissociation of H_2 molecules on the material's surface. A conversion of this H_2 gas to hydrogen plasma beforehand increases the hydrogen fugacity and makes it possible to evaluate hydrogen embrittlement inside the ESEM. Hence, Wan et al. [22] combined an in-situ slow strain rate tensile test together with in-situ hydrogen plasma charging inside an ESEM. A ductility loss of about 5% was obtained and fractographic analysis revealed clearly the hydrogen induced brittle features on the fracture surface. This type of approach was until recently only a few times considered. Hydrogen glow charging was for instance used on single crystals by Narita [23], who demonstrated that this method is able to charge the material with hydrogen to evaluate the hydrogen embrittlement sensitivity without damaging the sample during charging. On the contrary, a softening in the flow stress of pure iron samples due to hydrogen plasma charging was observed by Kimura and Birnbaum [24]. All in all, this methodology offers opportunities to have a direct observation during tensile testing while in-situ hydrogen plasma charging is applied. Comparison with traditional electrochemical charging on the same material has not yet been performed to verify the effective hydrogen effect on the mechanical properties. Therefore, we will use the same established methodology as in Ref. [22] in the current work on a DP steel grade.

This DP steel has been subject of many recent works [25, 26, 27, 28, 29, 30]. The material microstructure, consisting of a ferritic matrix with martensitic islands, makes them attractive materials for automotive applications due to their good combination of strength and ductility. The typical characteristics are realized by its thermo-mechanical processing and the volume fraction of austenitic islands that transform into martensite. The strength level is principally dependent on the volume fraction and hardness of the martensite in the DP

microstructure. A uniform distribution of martensite showed a slower rate of damage growth in non-hydrogen charged conditions, whereas center-lined martensite formation exhibited accelerated void growth and therefore detrimental significances [31]. Nevertheless, the significant mechanical contrast between both phases (i.e. ferrite and martensite) come with certain risks, i.e. severe strain/stress partitioning, strain localization and damage evolution, for instance by martensite cracking. Unfortunately, the risk for these potential issues is even increased in the presence of hydrogen.

The automotive industry is endeavoring to lower vehicle weight in order to diminish fuel consumption and to meet the stringent CO_2-emission protocols while an increase in strength and stiffness level is also relevant due to more stringent safety regulations. Outstanding candidates to accomplish these requirements are advanced high strength steels. However, these grades are unfortunately more prone to hydrogen embrittlement. BMW therefore even doubts the use of high-strength materials for automotive applications as they point out that steels with a tensile strength above 1000 MPa, may fail due to hydrogen embrittlement which impedes the use of the highest strength steels for body-in-white applications [32]. Among the advanced high strength steels, DP, TRIP, complex phase (CP), HSLA and martensitic steels are the main ones. The hydrogen embrittlement sensitivity of these materials was evaluated by Depover et al. [33] and they demonstrated that HSLA steel showed the highest resistance to cathodic hydrogen charging till saturation with a hydrogen induced ductility loss of about 8%. The present carbides were assumed to play a beneficial role in improving the resistance. DP steel embrittled with 54%, while TRIP lost 60% of its ductility. DP steel was also subject of another study, where the fractography was evaluated thoroughly [30]. The hydrogen penetration depth from the edges, based on hydrogen diffusivity laws, was clearly visualized since a transition from a hydrogen induced embrittled zone to a ductile central area was revealed exactly at this penetration depth. Koyama *et al.* [25] investigated the micro-cracking behavior in martensite-ferrite DP steels in the presence of hydrogen. They clearly observed that hydrogen influenced considerably the damage evolution process. Basically, they concluded that both the hydrogen-enhanced decohesion (HEDE) and hydrogen-enhanced localized plasticity (HELP) mechanisms contributed to the damage evolution in DP steels leading to an unpredictable hydrogen induced failure.

The aim of this work is to gain insight in the hydrogen embrittlement behavior of DP steel by observing the hydrogen effect by in-situ hydrogen plasma charging. The plasma charging will be compared with conventional electrochemical charging and both will be compared with reference tensile tests performed without hydrogen. Fractography will help elucidating the obtained hydrogen induced ductility loss and will reveal the impact of the different hydrogen charging procedures on the tensile specimen. This comparison will serve as a validation for the plasma charging procedure used by Wan et al. [22]. The effect of cold deformation and hence the increase in dislocation density is aimed to be assessed, since dislocations are known to play a decisive role in the hydrogen embrittlement in specific cases [20, 34, 35, 36, 37, 38].

2. Experimental procedure

Hydrogen induced mechanical degradation of DP600 steel will be studied in this work. Hot and cold rolling was done till a final thickness of 1.2 mm, which was followed by subsequent annealing via industrial annealing parameters required to obtain the desired microstructure, i.e. a ferrite-martensite combination. The chemical composition of the considered grade is presented in Table 1. Deformation of 15% was applied by cold rolling on the material in order to increase the dislocation density, because of its relevance in the hydrogen related failure.

Consequently, two different conditions are compared with each other: the as-received condition (DP 0%) and the cold deformed (DP 15%) condition.

Electron backscatter diffraction (EBSD) was performed to get a quantitative indication on the increase in dislocation density by the applied deformation. The examinations were executed on the transversal direction plane. The samples were ground and polished up to 1 μm, followed by an additional step using colloidal silica (Struers OPU suspension). This final step was performed long enough to remove the layers affected by polishing with coarser particles. The SEM utilized for EBSD measurements was an FEI Quanta 450 with field emission gun (FEG). The following settings were applied: acceleration voltage of 20 kV, emission current of 200 μA, specimen tilt of 70° and a scan step size of 80 nm on a hexagonal scan grid. In this study, the Geometrically Necessary Dislocation (GND) density was calculated by the TSL-OIM Data Analysis V7 software. The GND density was calculated using local misorientations below 5° and a second neighbor misorientation averaging. Before determination of the GND density, a clean-up procedure of neighbour confidence index (CI) correlation was applied. CI quantifies the reliability of the pattern indexation and the minimum was set at 0.1. As such, a partition was obtained from which the martensitic islands were removed. Hence, the GND density in the ferritic grains could be determined.

Table 1: Chemical composition of DP600 steel in wt%.

Material/Element	C	Mn	Si	Cr + Mo	Other
DP steel	0.07	1.50	0.25	0.4-0.8	200-250 ppm Al, 10-15 ppm S, 10-20 ppm P, 15-20 ppm N

Tensile samples were machined by waterjet cutting with their tensile axis along the rolling direction. A dogbone-shaped specimen was used with gauge geometry of 5 mm x 2 mm x 0.6 mm, as illustrated in Figure 1. Grinding to #4000 emery paper was followed by 3 μm and 1 μm diamond paste polishing. Subsequently, electropolishing was done to assure a smooth surface finish without residual deformation. The sides of the samples were grinded and subsequently polished as well. The tensile module from Kammrath & Weiss GmbH was used to perform the mechanical tests inside a Quanta 650 ESEM. An engineering strain rate of 10^{-4} s^{-1} was chosen in order to give hydrogen plasma sufficient time for adsorption, absorption and diffusion. Hydrogen plasma charging was done using an Evactron Model 25 Zephyr Plasma Cleaner with gaseous H_2 as process gas from a hydrogen generator. The plasma source was operated at a forward power of 14 W at 13.56 MHz maximum and a reverse power of 0.5 W. A constant gaseous hydrogen flow rate of 250 ml/min from the hydrogen generator was used as the source gas. The pressure in the ESEM chamber was around 40 Pa and the working pressure increased to 80 Pa when plasma was excited. These conditions are similar to the ones used by Wan et al. [22]. Vesel et al. [39] measured a density of hydrogen atom of about 2.5×10^{21} atom/m^3 in comparable plasma formation conditions. This shows that atomic hydrogen is the main expected constituent of the plasma in the vicinity of the source. The fugacity of dissociated hydrogen atoms will be far above 80 Pa, as reported by Bond et al. [40] and can reach values as high as several MPa. According to the conclusions in Ref. [41], hydrogen embrittlement does not occur with insufficient hydrogen concentration. Therefore, the hydrogen amount in this work showed to be enough to cause hydrogen induced degradation (cf. section 4). Furthermore, the interaction of plasma with the materials happens at a location remote from the plasma glow. The surface is thus prevented from heating, contaminating and damaging effects. The experimental setup in the ESEM chamber is illustrated in Ref. [22]. Hydrogen plasma charging was done for 2 hours and continued during the tensile test.

For sake of comparison with a more established conventional hydrogen charging method, tensile tests were also performed after electrochemical hydrogen charging. Charging was done in a borax/glycerol based electrolyte [42] at a current density of 10 mA/cm^2 for 2 hours. After hydrogen charging, tensile specimens were put within 2 minutes in the ESEM chamber and the same tensile test was performed, without the application of plasma charging. Both hydrogen charging procedures, i.e. in-situ plasma charging and electrochemical cathodic charging, are compared with tensile tests done without any hydrogen charging. Consequently, the effect of electrochemical hydrogen charging, which is well-known, can be compared with the novel hydrogen plasma charging procedure. All tests were done under the same vacuum condition in the ESEM.

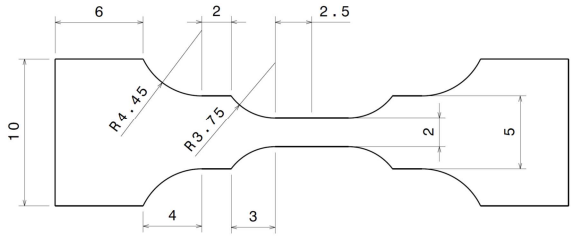

Figure 1: Tensile sample geometry in mm (thickness = 0.6 mm).

The effect of both hydrogen charging procedures on the mechanical properties is evaluated by comparing the observed stress-strain curves with tensile tests performed without hydrogen charging. The corresponding degree of hydrogen induced mechanical degradation was determined as defined in Equation 1, with ε_{ch} and ε_{un} being the total elongation of the hydrogen charged and uncharged tensile sample, respectively. Hence, the %HE varies between 0 and 1, with 0 meaning that there is no ductility loss and the material is insensitive to HE. When an index of 1 is obtained, the ductility drop is 100% and HE is maximal.

$$\%HE = 100 \cdot \left(1 - \frac{\varepsilon_{ch}}{\varepsilon_{un}}\right) \tag{1}$$

Complementary in-situ electrochemical nano-indentation tests were done to evaluate the hydrogen effect on the hardness of the materials. Hence, the impact of the modified dislocation density on the nanomechanical response could be assessed. These tests were done using a Hysitron TI 950 TriboIndenter® system with an integrated small-size electrochemical cell. Detailed information about the electrochemical cell integrated into the nano-indenter device can be found in [5]. The sample surface was prepared by grinding and polishing to 1 µm, followed by subsequent electropolishing, similarly as for the tensile specimens. The in-situ nano-indentation tests were done after cathodic charging in the same borax/glycerol solution and were compared with indents done in air. A conical indenter tip was used for the nano-indentation. The used load function consisted of a loading segment with a 8000 µN/s loading rate and a 0.5 s holding time at peak forces of 2000 µN and 2750 µN. The unloading rate was also at 8000 µN/s. The surface was always imaged using scanning probe microscopic imaging before and during charging to assure that the surface roughness remained intact upon charging, ensuring reliable nanomechanical data. The measured load-displacement curves were analyzed to extract the hardness [43], as given in Eq. 2. P_{max} is the maximal applied load, while A_c is the projected contact area evaluated from the contact depth and the tip area function.

$$H = \frac{P_{max}}{A_C} \tag{2}$$

Further characterization on the amount of charged hydrogen was only done for the electrochemically charging condition, due to practical reasons. Thermal desorption spectroscopy (TDS) was first done to identify both the

hydrogen trapping sites and their corresponding activation energy. Therefore, three different heating rates were used (200°C/h, 600°C/h and 1200°C/h). The samples were analysed about two minutes after hydrogen charging, similarly as the tensile tests. To determine the activation energy (E_a) of hydrogen traps related to the peaks observed in the TDS spectra, the method based on the work of Lee et al. [44, 45, 46] was used. Equation (3) is a simplification of the original formula of Kissinger [47], where Φ is the heating rate (K/min), T_{max} (K) the TDS peak temperature, E_a (J/mol) the detrapping activation energy for the specific H trap associated with T_{max} and R ($JK^{-1}mol^{-1}$) the universal gas constant. After TDS measurements were performed using different heating rates, the spectra were deconvoluted and the corresponding peak temperatures for a trap were determined. Plotting $\ln(\Phi/T_{max}^2)$ vs. $(1/T_{max})$ allows to obtain the E_a corresponding to that specific trap.

$$\frac{d(\ln\frac{\Phi}{T_{max}^2})}{d(\frac{1}{T_{max}})} = -\frac{E_a}{R} \quad (3)$$

Additionally, hot extraction was performed to determine the hydrogen content. The samples were analysed also about two minutes after hydrogen charging and the measurements were done at 300°C to determine the diffusible hydrogen content, similarly as in our previous work. The system comprises an infrared furnace in which a pre-weighted sample is heated. At this temperature, the metallic sample is heated and releases its hydrogen as gaseous H_2. The latter is taken up by a nitrogen flow and the mixture (N_2–H_2) is sent to a thermal conductivity measuring cell. The thermal conductivity of the mixture depends on the H_2 concentration because of the significant difference in conductivity of H_2 and N_2. The software calculates the hydrogen concentration of the sample based on the thermal conductivity variation and appropriate calibrating.

3. Materials characterization

The as-received DP600 steel is a ferritic-martensitic dual phase steel with approximately 23.6% of martensite. The corresponding grain sizes were about 7 µm for the ferritic phase and about 2 µm for the martensitic phase, as shown in Figure 2. Cold deformation clearly induced slip bands in the ferritic grains, based on the image quality maps shown in Figure 2. Applying deformation should result in an increase in dislocation density [20, 48, 49]. This was evaluated by determining the GND, as described in the experimental procedure. The ferritic grains were considered by making a partition in the EBSD data with CI > 0.1. As such, the martensitic islands are excluded from the GND determination of the ferritic grains. The results are presented in Table 2. A significant increase, about doubling, in dislocation density was observed in the ferritic grains due to the applied deformation of 15%.

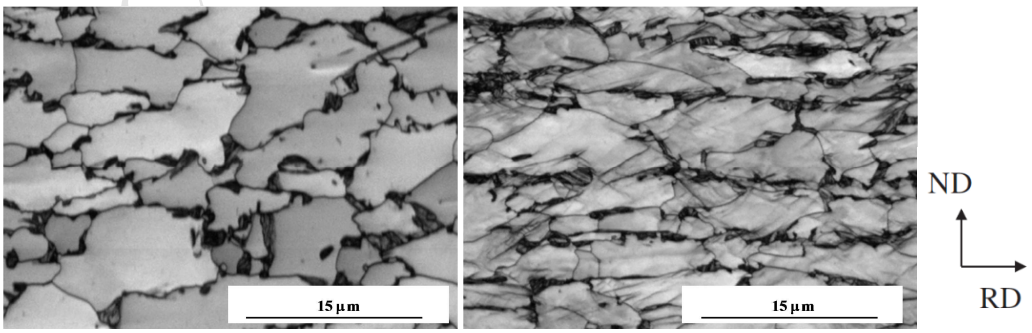

(a) (b)

Figure 2: Image quality map obtained by EBSD analysis of the as-received DP 0% (a) and cold deformed DP 15% (b) material. Rolling direction (RD) and normal direction (ND) is indicated.

Table 2: Geometrical necessary dislocation (GND) density for DP 0% and DP 15%

Material	GND density (10^{12} m^{-2})
DP 0%	108
DP 15%	192

4. Hydrogen induced mechanical degradation

Two material conditions (DP 0% and DP 15%) were evaluated under two different hydrogen charging conditions, i.e. in-situ plasma charging and electrochemical charging in the borax/glycerol solution. Both charging conditions were compared to tensile tests performed without hydrogen charging. Tests were at least performed twice to check the reproducibility. The corresponding stress-strain curves are presented in Figure 3. The related degree of hydrogen embrittlement is summarized in Table 3. When considering the tests performed without hydrogen charging, a yield strength of about 350 MPa (0.2% offset) and ultimate tensile stress of 600 MPa is obtained for DP 0%. This is in good agreement with previous reported results on this grade [30] and typical for DP materials in general. When 15% of cold deformation was applied, the yield strength increased significantly, together with a decrease of ductility. Both can be linked to the increase in dislocation density, resulting in a harder material and as confirmed by the GND determination (cf. Table 2).

When the materials were charged in-situ with plasma, a rather limited effect of hydrogen was observed. The strength level increased slightly, while ductility was only reduced to a small extent for DP 0%. A similar although consistently larger effect on both the strength level and obtained ductility was observed for DP 15%. These results were correlated to the specimens which were charged electrochemically prior to tensile testing. Similar findings were obtained since strength level was increased while ductility was reduced due to hydrogen charging. This tendency was again more pronounced when cold deformation was applied (DP 15% vs. DP 0%). The effect of the strength level was however more persistent for plasma charging whereas the effect on ductility was higher for electrochemical charging procedure. A slight hardening effect due to plasma charging was also observed by Wan et al. [22]. Similar hardening effect on the yield strength due to electrochemical hydrogen charging was also reported in [33, 50]. The effect seems to be larger when in-situ plasma charging is done, as this implies the continuous supply of plasma during tensile test. This hydrogen source was absent during deformation when the sample was charged ex-situ electrochemically. As in-situ plasma charging continues during deformation, which is concentrated at the surface of the specimen, the effect on the yield strength is more pronounced. The increase of the yield strength and flow stress can be attributed to solid solution strengthening by hydrogen, as hydrogen might pin the dislocations [38, 51, 52, 53]. This will be further evaluated by in-situ nanomechanical indentation. Also the different impact of both charging procedures on hydrogen induced ductility loss will be addressed further when considering the hydrogen trapping capacity and the fractography of the tensile specimens. However, based on the obtained degrees of hydrogen embrittlement as summarized in Table 3, it was observed that electrochemical charging deteriorated the materials' ductility more than plasma charging and that the hydrogen effect was generally more pronounced for DP 15%, probably due to the deformation induced defects, as discussed in the following section.

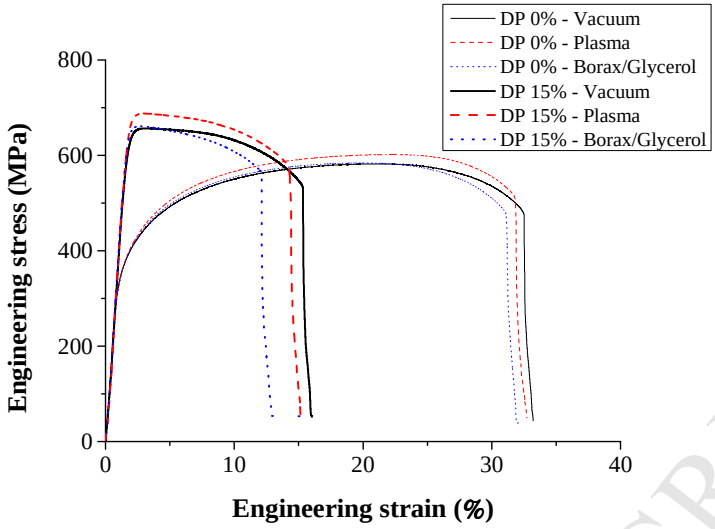

Figure 3: Stress-strain curves for DP 0% and DP 15% in the uncharged (vacuum), hydrogen plasma charged and electrochemically hydrogen charged condition.

Table 3: Summary of the HE degree of DP 0% and DP 15% for plasma and electrochemical charging.

HE (%)	Plasma	Borax/Glycerol
DP 0%	2	4
DP 15%	5	19

The impact of hydrogen was also verified by in-situ electrochemical nano-indentation tests. The nanomechanical response of individual ferritic grains were tested since these grains underwent the cold deformation and showed an increased dislocation density (cf. Figure 2 and Table 2). The corresponding load-displacements curves of multiple indents at peak force of 2000 µN, both in air and during in-situ hydrogen charging, are presented in Figure 4 (a). When considering the tests performed in air, a lower displacement was found for DP 15% due to its increased dislocation density and hence higher hardness level. Hydrogen charging resulted in decreased indentation depth for both conditions. The effect was, however, more persistent when deformation was performed. To evaluate the hydrogen effect at the same indentation depth for both DP 0% and DP 15%, the force peak level was increased to 2750 µN for the DP 15% material. As such, the air tests contained the same displacement and the effect of hydrogen could be assessed with the same reference condition. The related force-displacement curves are shown in Figure 4 (b). A similar tendency was found and the hardness values were determined according to Eq. 2 and represented in Figure 5. At first, the hardness level was significantly increased for DP 15% due to the increased dislocation density. Secondly, the effect of hydrogen was clearly more pronounced for DP 15% compared to DP 0%. This hardening effect was also observed in the stress-strain curves (cf. Figure 3) and the increased dislocation density can be set responsible for this. Since the effect is larger for DP 15%, the hydrogen/dislocation interaction is clearly responsible for this hardening effect, confirming the dislocation pinning effect by hydrogen.

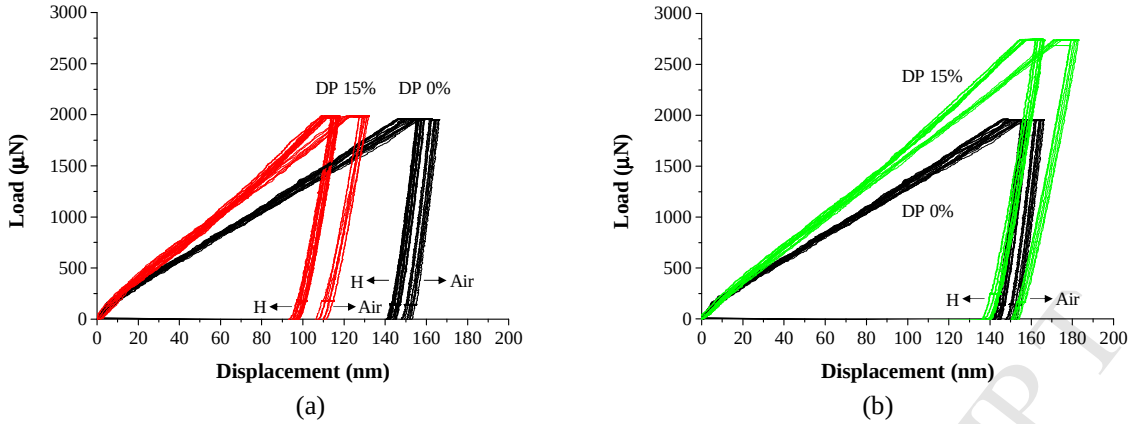

Figure 4: Representative load-displacement curves for DP 0% (black) and DP 15% (red) in air and during in-situ hydrogen charging (bolt) at peak force of 2000 µN (a). Peak force was increased to 2750 µN for DP 15% (green) to evaluate the hardness increase due to hydrogen (b).

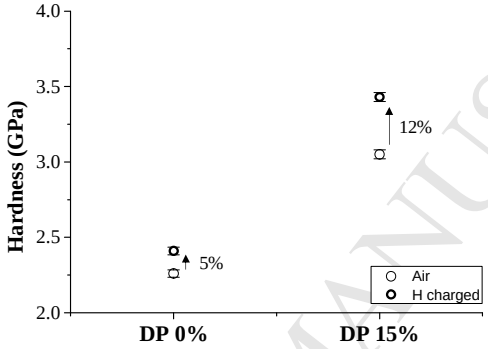

Figure 5: Hardness determination for DP 0% and DP 15% in air and during in-situ hydrogen charging based on the nanomechanical load-displacement curves obtained from Fig. 4 (b).

5. Evaluation of the applied deformation on the hydrogen trapping capacity

The hydrogen related characterization was performed for the samples which were electrochemically charged in the borax/glycerol based electrolyte to have an indication on the amount of (diffusible) hydrogen and the available hydrogen trapping sites. The actual hydrogen content was determined by hot extraction, as shown in Figure 6 (a). The results showed that saturation was reached after two hours of charging and that rather low amounts of hydrogen were found. When the same material was charged in a H_2SO_4 based electrolyte, considerably higher amount of diffusible hydrogen (2.32 wppm) was obtained, which consequently resulted in an increased hydrogen induced ductility loss [30, 33]. The rather low hydrogen amount charged into the materials can be held responsible for the limited observed HE% (cf. Table 3). However, the use of the glycerol/borax electrolyte was opted for this study to allow a comparison with the plasma charging method, for which quite similar results were found. In addition, the surface condition is also unaffected by the glycerol/borax solution, as demonstrated by Hajilou et al. [42], compared to severe charging by the sulphuric acid based electrolyte. This allows a direct observation without additional surface polishing inside the ESEM chamber. The use of an acidic solution would deteriorate the surface state significantly. Furthermore, the reduced resistance against hydrogen embrittlement for DP 15% compared to DP 0% is in correspondence with the higher amount of diffusible hydrogen charged in the cold deformed material. Next to the effective amount of hydrogen charged into the material, also the effective hydrogen trapping site(s) plays a crucial role to understand the observed hydrogen embrittlement degrees.

Therefore, TDS was done for both DP steel conditions (cf. Figure 6 (b)). Since detection of hydrogen can be done two minutes after charging, the TDS setup is able to capture the mobile hydrogen, mostly trapped by dislocations, as well, which is a main advantage of this TDS device as compared to the other TDS device used in previous work [20, 54]. The corresponding spectrum at a heating rate of 600°C/h is shown in Figure 6 (b). Firstly, DP 15% contained more H compared to DP 0% as was also seen by hot extraction. Secondly, a distinct shoulder in the beginning of the spectrum is clearly observed when cold deformation was applied. Only a limited indication for this shoulder is detectable for DP 0%. Depover et al. [20] recently correlated this first shoulder in the TDS spectrum to hydrogen trapped by dislocations by varying the deformation degree in Fe-C-X alloys. This indicates that the deformation induced defects such as dislocations, represented by the increase in GNDs, were able to weakly trap hydrogen. Finally, the TDS peak of DP 15% is slightly shifted to higher temperatures and hydrogen peak values, which can be related to a decrease in hydrogen diffusivity caused by the applied cold deformation [20, 49, 55]. Consequently, more hydrogen is trapped at dislocations for DP 15%. This hydrogen has been confirmed to play a detrimental role in hydrogen embrittlement, which has been associated with the HELP mechanism [20]. Deconvolution of the DP 15% TDS spectrum into two separate peaks enables to determine the corresponding activation energies, based on the Kissinger Equation. Peak 1 corresponds to an E_a of about 25 kJ/mol and with hydrogen trapped at dislocations. Similar E_a 's for hydrogen trapped at dislocations were obtained in other studies [7, 55, 56, 57]. The second peak with an E_a of about 30 kJ/mol is linked to the grain boundaries [58] in the dual phase microstructure.

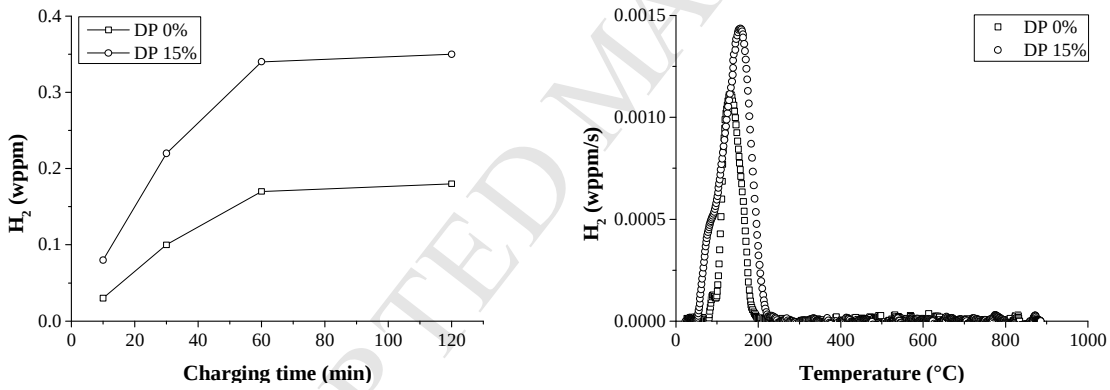

(a) (b)

Figure 6: Hot extraction results versus applied charging time for DP 0% and DP 15% (a). TDS spectra for DP 0% and DP 15 % at a heating rate of 600°C/h.

6. Fractographic analysis

Despite the fact that only a limited, yet consistent effect of hydrogen was observed in the stress-strain curves, an increased hydrogen effect was present when deformation was applied for both charging procedures. This was associated to the increased density and the specific trapping ability of the dislocations, as demonstrated above. The fracture surfaces of the tensile specimens were also analyzed to further verify and validate the impact of hydrogen for both charging procedures. Direct ESEM observation enabled to capture the fracture initiation to occur from the center of the sample (cf. Figure 7 (a)), indicating a ductile failure mode affected by the high stress triaxiality in the center of the tensile sample [59]. Figure 7 (b) presents the fracture surface of DP 0%, charged electrochemically with hydrogen. The white arrows indicate the hydrogen induced brittle area, whereas the central zone failed by ductile microvoid coalescence. The hydrogen affected regions on the fracture surfaces for all conditions were determined, as shown in Figure 8. From the edges onwards, a hydrogen embrittled, more or

less rectangular, area can be identified. The corresponding distances, from both top/bottom and left/right, are summarized in Table 4. The distances of the hydrogen affected regions corresponded well to the observed degrees of hydrogen embrittlement (cf. Table 3), which confirms the hydrogen impact on the mechanical properties. Representative detailed ESEM images of the brittle and ductile regions on the fracture surface of DP 15% are shown in Figure 9. As hydrogen might effuse from the samples during the tensile test in the case of electrochemical charging, the hydrogen induced brittle area can also be correlated to the hydrogen diffusivity. Besides the higher amount of hydrogen for DP 15%, also its hydrogen diffusivity is lower due to the increased dislocation density. In addition, this material condition showed a lower testing, and hence decreased hydrogen effusion, time compared to DP 0%. This might account for the increased hydrogen induced brittle area for DP 15%. This diffusivity effect does, however, not play a role when plasma charging was applied, since plasma charging continued during the test.

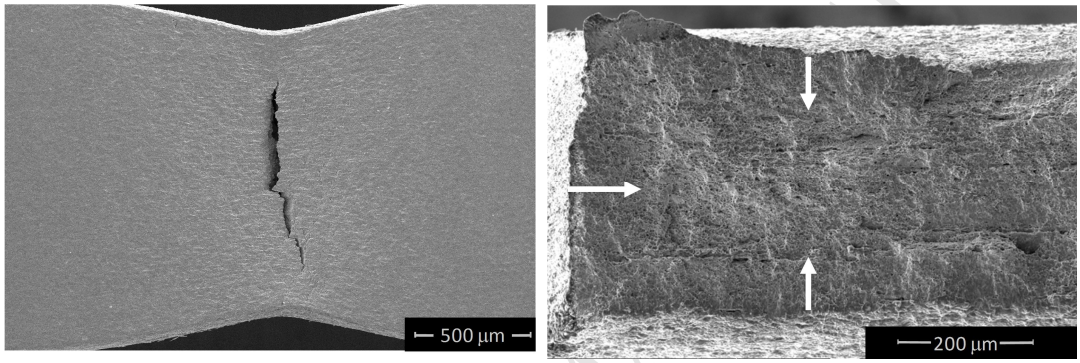

(a) (b)

Figure 7: ESEM images of side view (a) and fracture surface (b) of DP 0% charged electrochemically. The arrows indicate the hydrogen affected zone.

	Electrochemical charging	**Plasma charging**
DP 0%	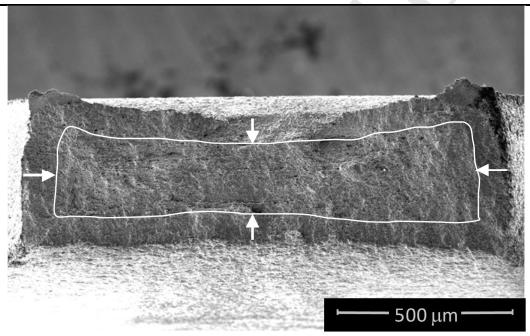	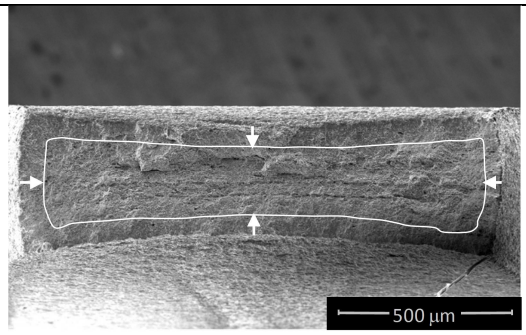
DP 15%	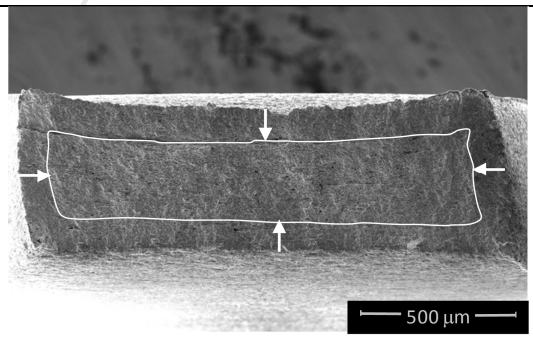	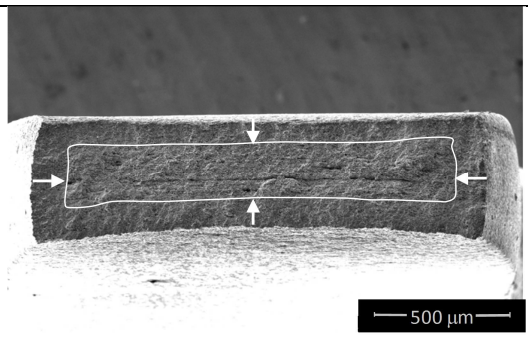

Figure 8: ESEM images of the fracture surfaces of DP 0% and DP 15%, both charged electrochemically in borax/glycerol and by hydrogen plasma.

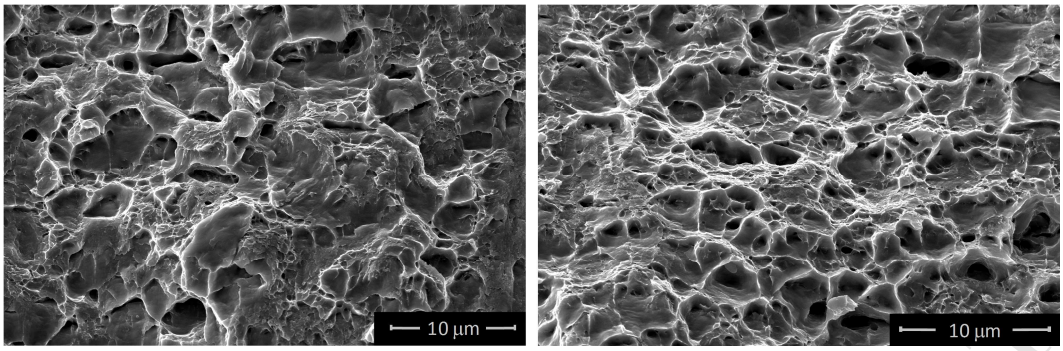

(a) (b)

Figure 9: High magnification ESEM images of DP 15% charged electrochemically revealing the brittle (a) and ductile (b) regions in detail.

H affected zone (µm)	Borax/glycerol		Plasma	
	⇄	⇅	⇄	⇅
DP 0%	100 ± 6	80 ± 6	70 ± 5	60 ± 5
DP 15%	120 ± 8	110 ± 7	110 ± 7	95 ± 6

Table 4: Summary of the hydrogen affected regions based on Figure 8.

In addition, a peculiar line is observed in the samples' center for all conditions, even the one without hydrogen charging. This is a result of the segregation line which typically is present for DP steels. Impurities, such as S, tend to segregate in this central line, forming MnS inclusions. In the presence of H, these MnS inclusions can initiate H induced cracking [60]. This has been shown for this DP steel in previous research [2, 30, 59]. Figure 10 shows a detailed image of this central line for the uncharged, electrochemical charged and plasma charged condition of DP 0%. Especially when charged with borax/glycerol, a distinct embrittled crack is revealed, where MnS inclusions were found in [30, 59]. Figure 11 illustrates the presence of these inclusions in the H induced crack in the central segregation line, as reported in [59]. Since saturation over the entire thickness was confirmed for the electrochemical charging procedure (cf. Figure 6 (a)), hydrogen is present in this central line, and will cause hydrogen induced cracking. In the case of plasma charging, a limited and rather similar effect on this central line is observed as compared to the uncharged condition. Therefore, one could assume that plasma charging mainly charges the surface and subsurface areas. During the necking stage, hydrogen plasma continues charging the material, which increases its penetration depth. However, these results indicate that plasma charging might not have saturated the entire specimen, which was clearly the case for the samples charged electrochemically (cf. Figure 6(a)). Consequently, this might account for the increased hydrogen induced ductility loss for the samples charged electrochemically compared to plasma charged specimens (cf. Figure 3).

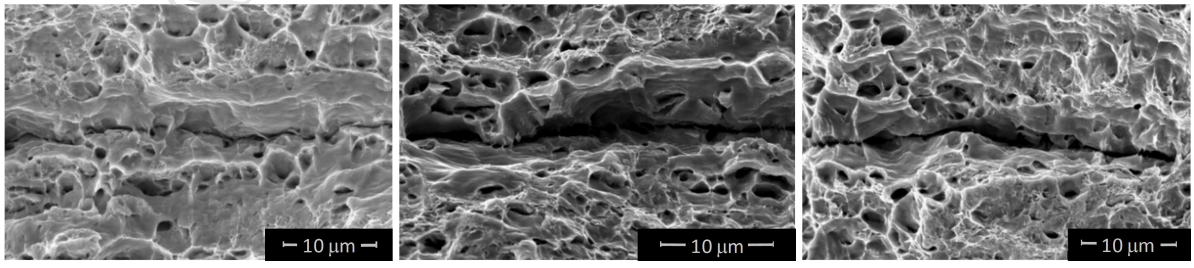

(a) (b) (c)

Figure 10: SEM images of fracture surface at the central embrittled line for the (a) uncharged, (b) electrochemically hydrogen charged and (c) hydrogen plasma charged tensile specimen.

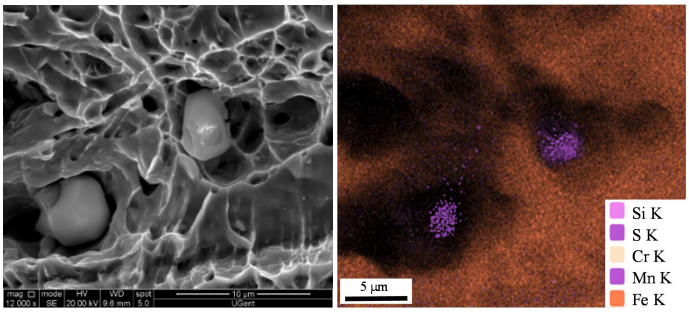

(a) (b)

Figure 11: SEM image (a) of MnS inclusions in the hydrogen induced crack observed in the central segregation line on the fracture surface of hydrogen charged DP steel, revealed by EDX analysis (b) [59]**.**

7. Conclusion

The present work evaluated the hydrogen induced ductility loss in DP steel by performing small scale tensile tests inside an ESEM chamber. Cold deformation of 15% was performed to induce microstructural defects, resulting in an increased dislocation density, and to verify their effect on the obtained hydrogen embrittlement susceptibility. Hence, two material conditions, i.e. DP 0% and DP 15%, were considered. In-situ hydrogen plasma charging was compared with electrochemical hydrogen charging whereas uncharged samples were used as a reference. The impact of hydrogen on the mechanical properties, both on ductility as stress, increased with cold deformation. Thermal desorption spectroscopy demonstrated that this effect was correlated to the hydrogen trapping ability of the deformation induced defects, i.e. a higher dislocation density was obtained after cold deformation. The more pronounced hardness increase due to hydrogen was verified by in-situ electrochemical nanoindentation. Furthermore, a rather small increase in hydrogen embrittlement sensitivity was found when the samples were charged electrochemically compared to hydrogen plasma charging. However, quite similar tendencies were observed for both charging procedures. Direct ESEM observation of the fractography confirmed the observations since the distances of the hydrogen affected regions corresponded to the obtained degrees of hydrogen embrittlement. In addition, the detrimental role of MnS inclusions in the segregation line on hydrogen induced cracking was only clearly witnessed for the electrochemical charging procedure, which indicates that plasma charging is mainly acting on the surface and subsurface of the tensile specimen.

Acknowledgements

TD holds a postdoctoral fellowship via grant nr BOF01P03516. The authors wish to thank the Special Research Fund (BOF), UGent (BOF15/BAS/06). The authors also acknowledge the technicians and staff working at the Department Materials, Textiles and Chemical Engineering, UGent, for their help with the experiments and/or sample preparation. TH, DW, DW and AB acknowledge the HyFlex project founded by RCN.

Data availability

The raw/processed data required to reproduce these findings cannot be shared at this time as the data also forms part of an ongoing study.

References

[1] Pérez Escobar D, Depover T, Wallaert E, Duprez L, Verhaege M, Verbeken K, „Thermal desorption spectroscopy study of the interaction between hydrogen and different microstructural constituents in lab cast Fe-C alloys," *Corrosion Science*, vol. 65, pp. 199-208, 2012.

[2] Pérez Escobar D, Miñambres C, Duprez L, Verbeken K, Verhaege M, „Internal and surface damage of multiphase steels and pure iron after electrochemical hydrogen charging," *Corrosion Science*, vol. 53, pp. 3166-3176, 2011.

[3] Venezuela J, Tapia-Bastidas C, Zhou Q, Depover T, Verbeken K, Gray E, Liu Q, Liu Q, Zhang M, Atrens A, „Determination of the equivalent hydrogen fugacity during electrochemical charging of 3.5NiCrMoV steel," *Corrosion Science*, vol. 132, pp. 90-106, 2018.

[4] Atrens A, Venezuela J, Liu Q, Zhou Q, Verbeken K, Tapia-Bastidas C, Gray E, Christien F, Wolski K, „Electrochemical and mechanical aspects of hydrogen embrittlement evaluation of martensitic steels," *Surface Science and Electrochemistry*, pp. 201-225, 2018.

[5] Barnoush A, Vehoff H, „Recent developments in the study of hydrogen embrittlement: Hydrogen effect on dislocation nucleation," *Acta Mat*, vol. 58, pp. 5274-5285, 2010.

[6] Hachet G, Metsue A, Oudriss A, Feaugas X, „Influence of hydrogen on the elastic properties of nickel single crystal: A numerical and experimental investigation," *Acta Mat*, vol. 148, pp. 280-288, 2018.

[7] Wei FG, Hara T, Tsuzaki K, „Precise determination of the activation energy for desorption of hydrogen in two Ti-added steels by a single thermal-desorption spectrum," *Met Mat Trans B*, vol. 35B, pp. 587-597, 2004.

[8] Pérez Escobar D, Wallaert E, Duprez L, Atrens A, Verbeken K, „Thermal Desorption Spectroscopy Study of the Interaction of Hydrogen with TiC Precipitates," *Met Mater Int*, vol. 19, pp. 741-748, 2013.

[9] Yamabe J, Takakuwa O, Matsunaga H, Itoga H, Matsuoka S, „Hydrogen diffusivity and tensile-ductility loss of solution-treated austenitic stainless steels with external and internal hydrogen," *Int Journal of Hydrogen Energu*, vol. 42, pp. 13289-13299, 2017.

[10] Ichii K, Koyama M, Tasan CC, Tsuzaki K, „Comparative study of hydrogen embrittlement in stable and metastable high-entropy alloys," *Scripta Mat*, vol. 150, pp. 74-77, 2018.

[11] Koyama M, Akiyama E, Lee YK, Raabe D, Tsuzaki K, „Overview of hydrogen embrittlement in high-Mn steels," *Int Journal of Hydrogen Energy*, vol. 42, pp. 12706-12723, 2017.

[12] Dadfarnia M, Sofronis P, Somerday BP, Balch DK, Schembri P, Melcher R, „On the environmental similitude for fracture in the SENT specimen and a cracked hydrogen gas pipeline," *Engineering Fracture Mechanics*, vol. 78, pp. 2429-2438, 2011.

[13] Martin ML, Somerday BP, Ritchie RO, Sofronis P, Robertson IM, „Hydrogen-induced intergranular failure in nickel revisited," *Acta Mat*, vol. 60, pp. 2739-2745, 2012.

[14] Deng Y, Hajilou T, Wan D, Kheradmand N, Barnoush A, „In-situ micro-cantilever bending test in environmental scanning electron microscope: Real time observation of hydrogen enhanced cracking," *Scripta Mat*, vol. 127, pp. 19-23, 2017.

[15] Rogne BRS, Kheradmand N, Deng Y, Barnoush A, „In situ micromechanical testing in environmental scanning electron microscope: A new insight into hydrogen-assisted cracking," *Acta Mat,* vol. 144, pp. 257-268, 2018.

[16] Depover T, Verbeken K, „Hydrogen trapping and hydrogen induced mechanical degradation in lab cast Fe-C-Cr alloys," *Mat Sci and Eng A,* vol. 669, pp. 134-149, 2016.

[17] Depover T, Verbeken K, „Evaluation of the role of Mo2C in hydrogen induced ductility loss in Q&T Fe-C-Mo alloys," *Int Journal of Hydrogen Energy,* vol. 41, pp. 14310-14329, 2016.

[18] Depover T, Verbeken K, „Evaluation of the effect of V4C3 precipitates on the hydrogen induced mechanical degrdation in Fe-C-V alloys," *Mat Sci and Eng A,* vol. 675, pp. 299-313, 2016.

[19] Depover T, Verbeken K, „The effect of TiC on the hydrogen induced ductility loss and trapping behavior of Fe-C-Ti alloys," *Corrosion Science,* vol. 112, pp. 308-326, 2016.

[20] Depover T, Verbeken K, „The detrimental effect of mobile hydrogen at dislocations on the hydrogen embrittlement susceptibility of Fe-C-X alloys: an experimental proof of the HELP mechanism," *Int Journal of H Energy,* vol. 43, pp. 3050-3061, 2018.

[21] Depover T, Van den Eeckhout E, Verbeken K, „Hydrogen induced mechanical degradation in tungsten alloyed steels," *Materials Characterization,* vol. 136, pp. 84-93, 2018.

[22] Wan D, Deng Y, Barnoush A, „Hydrogen embrittlement effect observed by in-situ hydrogen plasma charging on a ferritic alloy," *Scripta Mat,* vol. 151, pp. 24-27, 2018.

[23] Narita N, „Embrittlement of Fe-Si alloy crystals by hydrogen glow discharge," *Scripta Metall,* vol. 18, pp. 985-988, 1984.

[24] Kimura A, Birnbaum HK, „Plastic softening by hydrogen plasma charging in pure iron," *Scripta Metall,* vol. 21, pp. 53-57, 1987.

[25] Koyama M, Tasan CC, Akiyama E, Tsuzaki K, Raabe D, „Hydrogen-assisted decohesion and localized plasticity in dual-phase steel," *Acta Mat,* vol. 70, pp. 174-187, 2014.

[26] Liu Q, Zhou Q, Venezuela J, Zhang M, Atrens A, „The role of the microstructure on the influence of hydrogen on some advanced high-strength steels," *Mat Sci and Eng A,* vol. 715, pp. 370-378, 2018.

[27] Schaffner T, Hartmaier A, Kokotin V, Pohl M, „Analysis of hydrogen diffusion and trapping in ultra-high strength steel grades," *Journal of Alloys and Compounds,* vol. 746, pp. 557-566, 2018.

[28] Sun J, Jiang T, Sun Y, Wang Y, Liu Y, „A lamellar structured ultrafine grain ferrite-martensite dual-phase steel and its resistance to hydrogen embrittlement," *Journal of Alloys and Compounds,* vol. 698, pp. 390-399, 2017.

[29] Tasan C, Diehl M, Yan D, Bechtold M, Roters F, Schemmann L, Zheng C, Peranio N, Ponge D, Koyama M, Tsuzaki K, Raabe D, „An overview of dual phase steels: advances in microstructure-oriented precessing and micromechanicall guided design," *Ann Rev Mater Res,* vol. 45, pp. 391-431, 2015.

[30] Depover T, Wallaert E, Verbeken K, „Fractographic analysis of the role of hydrogen diffusion on the hydrogen embrittlement susceptibilty of DP steel," *Mat Sci and Eng A,* vol. 649, pp. 201-208, 2016.

[31] Avramovic-Cingara G, Ososkov Y, Jain MK, Wilkinson DS, „Effect of martensite distribution on damage

behaviour in DP600 dual phase steels," *Mat Sci and Eng A*, vol. 516, pp. 7-16, 2009.

[32] Loidl M, Kolk O, „Hydrogen embrittlement in HSSs limits use in lightweight body," *Advanced Materials and Processes*, vol. 169, pp. 22-25, 2011.

[33] Depover T, Pérez Escobar D, Wallaert E, Zermout Z, Verbeken K, „Effect of in-situ hydrogen charging on the mechanical properties of advanced high strength steels," *Int Journal of Hydrogen Energy*, vol. 39, pp. 4647-4656, 2014.

[34] Nagao A, Dadfarnia M, Somerday B, Sofronis P, O. Ritchie R, „Hydrogen-enhanced-plasticity mediated decohesion for hydrogen-induced intergranular and "quasi-cleavage"fracture of lath martensitic steels," *Journal of the mechanics and physics of solids*, vol. 112, pp. 403-430, 2018.

[35] Dadfarnia M, Martin ML, Nagao A, Sofronis P, Robertson IM, „Modeling hydrogen transport by dislocations," *Journal of the Mechanics and Physics of Solids*, vol. 78, pp. 511-525, 2015.

[36] Zhao K, He J, Mayer AE, Zhang Z, „Effect of hydrogen on the collective behavior of dislocations in the case of nanoindentation," *Acta Mat*, vol. 148, pp. 18-27, 2018.

[37] Leyson GPM, Grabowski B, Neugebauer J, „Multiscale modeling of hydrogen enhanced homogeneous dislocation nucleation," *Acta Mat*, vol. 107, pp. 144-151, 2016.

[38] Deng Y, Barnoush A, „Hydrogen embrittlement revealed via novel in situ fracture experiments using notched micro-cantilever specimens," *Acta Mat*, vol. 142, pp. 236-247, 2018.

[39] Vesel A, Drenik A, Zaplotnik R, Mozetic M, Balat□Pichelin M, „Reduction of thin oxide films on tungsten substrate with highly reactive cold hydrogen plasma," *Surface and Interface Analysis*, vol. 42, pp. 1168-1171, 2010.

[40] Bond GM, Robertson IM, Birnbaum HK, „On the determination of the hydrogen fugacity in an environmental cell TEM facility," *Scripta Metall*, vol. 20, pp. 653-658, 1986.

[41] Kimura A, Kimura H, „Hydrogen embrittlement in high purity iron single crystals," *Mat Sci and Eng* , vol. 77, pp. 75-83, 1986.

[42] Hajilou T, Hope MSB, Zavieh A, Kheradmand N, Johnsen R, Barnoush A, „In situ small-scale hydrogen embrittlement testing made easy: An electrolyte for preserving surface integrity at nano-scale during hydrogen charging"," *Int Journal of Hydrogen Energy*, 2018, accepted.

[43] Oliver W, Pharr G, „An improved technique for determining hardness and elastic modulus using load and displacement sensing indentation experiments," *Journal of Mater Res*, vol. 7, pp. 1564-1583, 1992.

[44] Lee JL, Lee JY, „Hydrogen trapping in AISI-4340 steel," *Metal Science*, vol. 17, pp. 426-432, 1983.

[45] Lee JY, Lee SM, „Hydrogen trapping phenomena in metals with bcc and fcc crystal structures by the desorption thermal-analysis technique," *Surface and Coatings Technology*, vol. 28, pp. 301-314, 1986.

[46] Lee SM, Lee JY, „The trapping and transport phenomena of hydrogen in nickel," *Met Trans A*, vol. 17A, pp. 181-187, 1986.

[47] Kissinger HE, „Reaction kinetics in differential thermal analysis," *Analytical Chemistry*, vol. 29, pp. 1702-1706, 1957.

[48] Porter DA, Easterling KE, Phase transformation in metals and alloys, London, UK: Chapman & Hall, 1992.

[49] Van den Eeckhout E, Laureys A, Van Ingelgem Y, Verbeken K, „Hydrogen permeation through deformed and," *Materials Science and Technology*, 2017, doi.org/10.1080/02670836.2017.1342015.

[50] Luo H, Li Z, Lu W, Ponge D, Raabe D, „Hydrogen embrittlement of an interstitial equimolar high-entropy alloy," *Corrosion Science*, vol. 136, pp. 403-408, 2018.

[51] Duprez L, Verbeken K, Verhaege M, „Effect of hydrogen on the mechanical properties of multiphase high strength steels.," in *Proc. of the 2008 Int. Hydrogen Conf.*, Jackson, Wyoming, USA, 2008.

[52] Depover T, Wallaert E, Verbeken K, „On the synergy of diffusible hydrogen content and hydrogen diffusivity in the mechanical degradation of laboratory cast Fe-C alloys," *Mat Sci and Eng A*, vol. 664, pp. 195-205, 2016.

[53] Hajilou T, Deng Y, Rogne BR, Kheradmand N, Barnoush A, „In situ electrochemical microcantilever bending test: A new insight into hydrogen enhanced cracking," *Scripta Mat*, vol. 132, pp. 17-21, 2017.

[54] Pérez Escobar D, Depover T, Wallaert E, Duprez L, Verbeken K, Verhaege M, „Combined thermal desorption spectroscopy, differential scanning calorimetry, scanning electron microscopy and X-ray diffraction study of hydrogen trapping in cold deformed TRIP steel," *Acta Mat*, vol. 60, pp. 2593-2605, 2012.

[55] Choo WY, Lee JY, „Thermal analysis of trapped hydrogen in pure iron," *Met Trans A*, vol. 13A, pp. 135-140, 1982.

[56] Hirth JP, „Effects of Hydrogen on the Properties of Iron and Steel," *Met Trans A*, vol. 11A, pp. 861-890, 1980.

[57] Pressouyre GM, „Classification of hydrogen traps in steel," *Met Trans A*, vol. 10A, pp. 1571-1573, 1979.

[58] Thomas LSR, Li D, Gangloff RP, Scully JR, „Trap-governed hydrogen diffusivity and uptake capacity in ultrahigh strength aermet 100 steel," *Met Mat Trans A*, vol. 33A, pp. 1991-2004, 2002.

[59] Depover T, Vercruysse F, Elmahdy A, Verleysen P, Verbeken K, „Evaluation of the hydrogen embrittlement susceptibility in DP steel under static and dynamic tensile conditions," *Journal of Impact Engineering*, vol. 123, pp. 118-125, 2019.

[60] Sasaki D, Koyama M, Noguchi H, „Factors affecting hydrogen-assisted cracking in a commercial tempered martensitic steel: Mn segregation, MnS, and the stress state around abnormal cracks," *Mat Sci and Eng A*, vol. 640, pp. 72-81, 2015.